Cellular Automata (Sandpile) models. Applications to Tokamak Plasmas and the Dynamics of Water Droplets.

James Anthony Merrifield

Abstract

This report concerns the development of two cellular automata sandpile models. The sandpile of *Chapman et al.* [14] was modified to be non-directed and to allow multiple feeding. A separate algorithm was devised to investigate the applicability of self-organised criticality (SOC) to the dynamics of water droplets on a "glass-like" inclined plane.

The time averaged height profile of the *Chapman et al.* sandpile has been shown to display some of the phenomenology of tokamak confined plasmas [10]. The simple modifications made to the *Chapman et al.* sandpile enabled further aspects of the sandpile's phenomenology to be identified with characteristic features of the tokamak temperature profile. These features are: the dependence of the position of "steps" and "plateaus" to the outflow boundary, the time signal of the electron temperature at a point of heating i.e. "giant saw-tooth crash", and the appearance of distinct peaks, termed "ears", when heating takes place at the edge of a "plateau".

The droplet model was developed in an attempt to understand how the dynamics of droplets could lead to the development of SOC. Concepts of threshold driven diffusion (redistribution by overcoming surface tension), non-threshold driven transport (fluid flow/diffusion), droplet formation on deposition and droplet formation in the wetted stream left by a moving droplet were introduced into the model. The statistics from the model were compared with those collected experimentally and qualitative agreement was found between them, particularly the statistics concerning the delay times between outflow events.

1. Introduction

Widespread interest in the statistical nature of sandpile models was sparked by the work of Bak, Tang and Wiesenfield (BTW) [1] in which they introduced the idea of Self-Organised Criticality (SOC). In this work, a computer model of an idealised sandpile was used to illustrate the vital principles of SOC. What follows in this section is a brief elaboration on two questions that naturally follow from the previous statements: (a) "Why is the study of SOC of interest?" and (b) "Why are computer models of sandpiles useful tools in the investigation of SOC"?

Self-organised criticality is a term used to describe complex systems that, seemingly contrary to the law of increasing entropy, evolve into a state of high order and behave very much like equilibrium systems at their critical point. However, systems for which SOC is applicable are often driven far from their equilibrium state. This critical state is characterised by the propagation of local distortions throughout the entire system, though direct interaction only takes place on a nearest neighbour level. The response of the system to perturbation is no longer accurately described by a characteristic length or time scale (i.e. an average consideration does not give a good description [2]). A lack of characteristic scale is described mathematically by power law scaling of the form:

$$N(A) \sim A^{-\alpha} \qquad (1)$$

Where $N(A)$ is the number of events of size A and α is a constant called the critical exponent.

Critical phenomena are well understood in equilibrium statistical mechanics with respect to phase transitions. A key difference between the equilibrium critical state and SOC is that SOC requires no fine-tuning of control parameters, where as the equilibrium critical state is only observed at specific temperatures and pressures.

Systems that evolve into a state described by SOC have a separation of time scales associated with them i.e. the driving process that may bring about an instability acts on a timescale much larger than instabilities relax. This is thought of as being due to the presence of thresholds and metastability. The development of scale-less dynamics (as described by (*1*)) and the development of order can be thought to come about in the following way:

Imagine a general system in which a potential is present at each site. A driving process tends to increase the potential at these sites. Once this potential exceeds a critical value, it is redistributed amongst other sites locally. The driving force slowly pushes many sites in the system towards instability. Many may remain in a state below the critical threshold (i.e. in a metastable state) but some may exceed this threshold leading to local redistribution by nearest neighbour effects. These nearest neighbour sites would then be pushed closer towards instability. Eventually a connected network of marginally sub-critical sites may form through which redistribution could be observed as a non-local phenomenon due to repeated nearest neighbour interaction. Such an "avalanche" is seen as one event macroscopically. Therefore, it is conceivable that events of any size may exist since the system may organise itself to possess connected networks on any scale. These networks do not exist in a temporally stable way because "avalanching events" destroy, as well as build these networks.

SOC combines the concepts of self-organisation and critical behaviour to explain complexity. The characterisation of complexity is discussed in [3]. A complex system is thought of as possessing a hierarchical structure. That is, it can be seen to consist of many similar interacting components (e.g. individual cars in a traffic jam) in which large scale events are a result of the repeated interaction of these components. Complexity research is concerned with showing that the behaviour of each level of the hierarchy is a macroscopic (or emergent) property of the level below it. As such, investigations that examine the universal macroscopic properties of these systems are favoured over those that examine all details. Complex systems that are thought to be examples of SOC include earthquakes, the development of river networks, propagation of forest fires and (controversially) evolution.

Sandpile models consist of a grid of cells, in which information about the pile's local height, or slope, are stored. The system is driven by the gradual addition of sand by a fuelling process. Once the local gradient exceeds some threshold value an avalanche is triggered and sand is redistributed. This redistribution could lead to further avalanches. Boundaries of the pile are either open (in which case mass loss events can take place) or closed (in which case any reference to cells that would lie outside this boundary are ignored). Sandpile models comply with the notions of complexity associated with SOC because:

- They consist of many locally interacting cells.
- They are maintained in a state far from equilibrium by constant fuelling and boundary interactions.
- There is a separation of time scales so that the system relaxes (completes a series of avalanches) far faster than the interval between fuelling events. This is important in allowing the critical state to evolve.

The list above, combined with the ease with which computer models allow data to be recorded and parameters to be controlled, makes the computer simulation of sandpiles an obvious tool in the investigation of SOC. An exact knowledge of the internal dynamics of the system inherent with computer simulation (in contrast to an experimental study of a sandpile) allows the application of the Renormalization Group (RG) [4][13]. RG is a powerful tool in predicting the large-scale behaviour of systems that exhibit self-similar dynamics. It provides the best way of determining *why* a system displays self-similarity and power law scaling.

2. Model Development and Behaviour

2.1 The Sandpile of Chapman et al.

2.1.2 Introduction

The study of sandpile models is an effective tool for assessing how useful the concepts of SOC are in explaining the dynamics of the temperature profiles of tokamak plasmas. Tokamaks are designed to confine plasmas at high enough temperatures to allow commercially viable nuclear fusion. They magnetically confine the plasma in a toroidal chamber so as to separate the plasma from the chamber wall [5][6]. The temperature profile of the tokamak plasma is essentially the distribution of plasma temperature, or electron energy, as a function of radial displacement within the toroidal chamber.

Two plasma energy transport mechanisms, for which a direct sandpile analogy exists, are diffusion and a phenomenon termed "avalanching". In this context, "avalanching" is a term used to describe the transport of energy in the plasma, which can occur on spatial scales up to the system size [9]. Mechanisms suspected of causing this transport only act on spatial scales of the order of ion gyroradii. In light of this, a transport mechanism that draws on the idea of SOC has been suggested [7]. This approach could explain this transport without a detailed consideration of the underlying transport mechanism [7] [8]. The local redistribution of sand, once a cell becomes over critical, is used as an analogy to diffusive transport and the "chain reaction" of local redistribution, which result in a sandpile avalanche, is used as an analogy to plasma "avalanching". It is appropriate to use the concept of a critical gradient to decide whether a cell is over critical or not because a critical gradient has been identified in the plasma temperature profile [7][8]. The fuelling cell of the sandpile model can be interpreted as the radial position at which the plasma is being heated and the open boundary is interpreted as the edge of the confinement chamber at which heat loss can occur. There is a table in [7] that lists the appropriate analogies that link transport mechanisms in sandpile models with turbulent transport in plasmas.

The *Chapman et al.* sandpile model is a one-dimensional model, and so consists of a row of cells. The update algorithm is a generalisation of that used by *P. Bak et al.* [1] so as to include a mechanism for the non-local redistribution of sand "uphill" from the avalanche site. This has a significant effect on the phenomenology of the model. The most readily obtainable result from the *Chapman et al.* model, which has direct relevance to tokamak plasma temperature profiles, is that of the average height profile of the sandpile. When this is averaged over many thousands of avalanches, after the system has evolved into the critical state, it displays steps and pedestals, which closely resemble those found in the temperature profiles of fusion experiments [10][11].

The aim of this investigation is to determine how much of the complicated behaviour displayed by tokamak confined plasmas can be reproduced with the sandpile of *Chapman et al.*

2.1.2 The Model of Chapman et al. and Model Development[1]

The original Chapman model is edge driven, so an amount of sand (γ) is periodically added to the cell next to the closed boundary (cell 1). Cell ***L*,** where **L** is the number of cells in the row, marks the last cell in the row, and thus

[1] The development of the *Chapman et al.* model was a task divided between the author and Mr. T. K. March. The principal results of this investigation (namely those presented in figures *1, 2* and 3) were obtained through development undertaken by Mr. T. K March. Their importance to the project warrants the inclusion of these results in this paper. Developments undertaken by the author concerned the introduction of a forward "fluidisation length".

the open boundary. The height of the pile at each cell is simply interpreted as the amount of sand in that cell (**h(k)** where k is the k^{th} cell) , which leads to following definition of the local gradient: $(k+1) - h(k)$. There is a gradient below which sand is always stable, c_r, and a gradient above which the sand is unstable and must be redistributed, c. Any further discussion of gradient will be in terms of C, which is defined by, $C = c_r - c$. Therefore, C is the gradient relative to c_r above which a cell is always unstable. The Chapman model is a generalised version of the BTW model to include a region of fluidisation (or non-local transport) "uphill" from the avalanche front to provide a mechanism for non-local redistribution of sand. Once the k^{th} cell becomes critical the following relaxation algorithm is applied:

$$h'(k+1) = h(k+1) + \Delta \qquad (2)$$

$$h'(k-i) = h(k-i) - \frac{\Delta}{L_f}, \qquad i = 0,\ L_f - 1 \qquad (3)$$

Where L_f is the fluidisation length and $h'(k)$ is the amount of sand in the k^{th} cell after one application of *(2)* and *(3)*. In terms of plasma analogy, L_f can be thought of as a turbulent correlation length or eddy size. The amount Δ is defined by the condition shown in *(4)*:

$$h'(k+1) - h'(k) = 0 \qquad (4)$$

Remembering a gradient of zero now represents the angle of repose. Note, *(2)* may cause the cell at k+1 to become unstable. Steps *(2)* and *(3)* are repeated until all cells are under-critical before sand is added at cell one again, i.e. relaxation is instantaneous. The entire process from cell one becoming critical to all cells being under-critical is defined as one avalanche. Mass loss events (MLEs) occur when cell L becomes critical and are handled by applying *(5)*.

$$h'(L-i) = 0 \qquad i = 0, L_f - 1 \qquad (5)$$

The behaviour of this model can be seen to be consistent with that of SOC when the elementary dissipative events are investigated. Power law scaling is found in the avalanche length distribution and the distribution of dissipated potential energy in avalanche events. For both cases $\alpha \approx 1$. This can be shown analytically, by exact solution for a limiting case [12] and generally through the application RG [13], and is found numerically [14]. The dissipated potential energy in an avalanche event, dE, is simply defined by *(6)*:

$$dE = \sum_{k=1}^{k=L} h^2(k)\Big|_{\text{before}} - \sum_{k=1}^{k=L} h^2(k)\Big|_{\text{after}} \qquad (6)$$

As such, the gravitational potential energy, E, of the system is then defined by *(7)*:

$$E = \sum_{k=1}^{k=L} h^2(k) \qquad (7)$$

In order to make the algorithm more physical, the critical gradient is not single valued but randomly fluctuates about a mean value ($\langle C \rangle$). Each cell has a critical gradient associated with it, C_k. A new critical gradient is chosen from a top hat distribution, which allows C_k to vary by 1% around $\langle C \rangle$, every time cell k becomes over critical. Results produced in [13] and [14] have been shown to be stable to these fluctuations.

The original Chapman model allows non-local redistribution to take place "uphill" of the avalanche front, but sand is only redistributed locally (to one cell) "downhill" from the avalanche front. It was decided to investigate the effect of allowing non-local redistribution to take place "downhill" from the avalanche front as well as "uphill" from it. This was designed to remove an asymmetry in the model that had no physical necessity. The control parameter L_{for} was used to control the range of non-local transport "downhill" from the avalanche front, in the same way as L_f is used to control the range of non-local transport "uphill" of the avalanche front. It was hoped that the introduction of this new parameter might change the way the system approaches its fixed point (as revealed by RG) or introduce a new non-trivial fixed point. The modified algorithm relaxes by steps (*2*) and (*3*), identically to the original algorithm. Two more stages follow:

$$h''(k+i) = h'(k+i) + \frac{\vartheta}{L_{for} - 1} \qquad i = 2, \quad L_{for} \tag{8}$$

$$h''(k-i) = h'(k-i) - \frac{\vartheta}{L_f + 1} \qquad i = -1, \quad L_f - 1 \tag{9}$$

Where h'' refers to the height of sand after this second relaxation process and h' still refers to the height of sand after an application of (*2*) and (*3*). Equation *(9)* removes an amount of sand, which totals to ϑ, from all cells that lie within the fluidisation region described by L_f and one cell that lies outside this region, i.e. cell k+1. Equation *(8)* then conservatively divides ϑ amongst all cells that lie within the fluid region described by L_{for} excluding cell k+1. ϑ was chosen to be proportional to $(L_{for} - 1)$, so $\vartheta = 0$ for $L_{for} = 1$ thus reducing the model back to its original form, and so that condition *(9a)* is satisfied, to parallel condition (3) on Δ. As such, ϑ is defined by *(9b)*.

$$h''(k+2) - h''(k+1) = 0 \tag{9a}$$

$$\vartheta = \frac{\left(h'(k+2) - h'(k+1)\right)\left(L_f + 1\right)\left(L_{for} - 1\right)}{L_f + L_{for}} \tag{9b}$$

2.1.3 Model Behaviour

The investigations below were designed to determine whether all the complicated phenomenology of tokamak plasmas can be recovered from the, reduced physics, sandpile model. If the sandpile model and the tokamak plasma are of the same universality class [20], then this should be possible.

An investigation was designed to determine whether the positions the stable plateauxs and "steps", common to both tokamak plasma profiles and the sandpile height profile, were determined by the position of the fuelling cell or the position of the open boundary. The model was generalised to enable avalanches to take place in both directions. Previously, because the pile was always fuelled from cell 1, avalanches could only propagate from lower to higher cell numbers. If the fuelling position is to be moved avalanches must be allowed to go both ways. A number of runs were performed with varying fuelling positions but with constant L_f (*see figure 1.)*. The boundary at L, here cell 1024, was closed and the boundary at cell 1 was open.

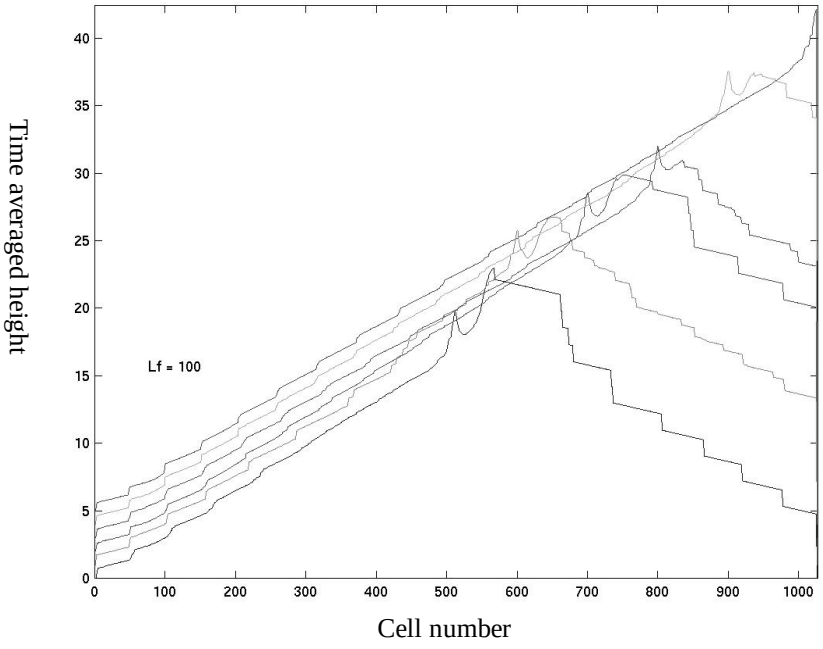

Figure 1: Average height profiles of 6 runs with $L_f = 100$ and varying fuelling cells. The boundary at cell 1 was open and the boundary at cell 1024 was closed. The "steps" near the open boundary seem to lie in the same position irrelevant of the fuelling cell.

It was found that the "steps" remained in broadly the same position suggesting that their positions are bound to the open boundary rather than the fuelling position of the fuelling cell.

"Giant saw-tooth crashes" are observed experimentally at sites of plasma heating. That is, the temperature of the plasma at a point of heating gradually increases with time and then drops suddenly to describe a saw-tooth like signal. The Chapman model was investigated in order to determine whether it describes this phenomenon. A method of visualising the evolution of the sandpile's height profile with time was developed using *Matlab*. This is a surface plot displaying height of sand on the vertical (z) axis and cell number and "time" on the x and y axis receptively. The amount of sand added to the pile is taken as a linear measurement of time since the same amount of sand is added periodically to the fuelling cell. Surface plots obtained show a clear saw-tooth crash effect at the fuelling cell (*see figure 2.).*

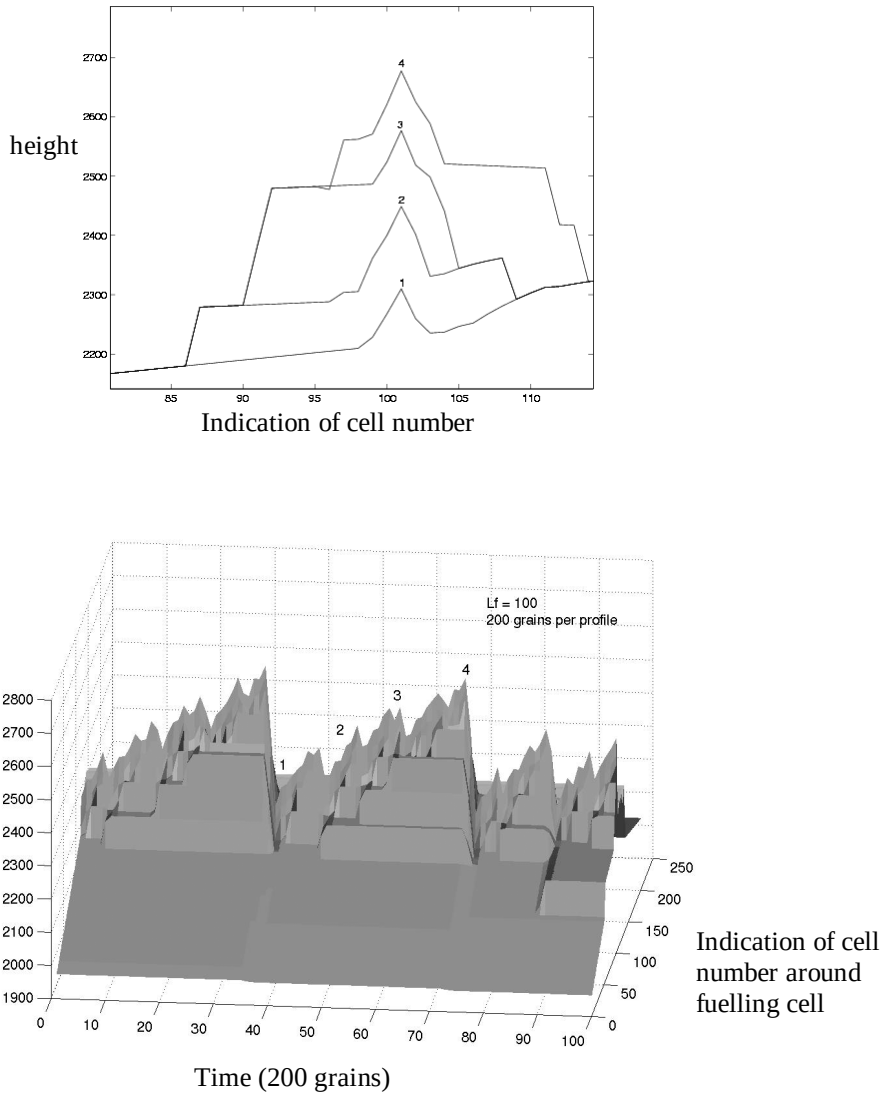

Figure 2: (Bottom) Surface plot to show saw-tooth like behaviour of the height at the fuelling cell with time. (Top) Cross-sectional slices to show the height profile around the fuelling cell at the times indicated by labels 1-4. $\mathbf{L_f}$ *was 100*

Tokamak plasmas that are heated at the centre of the toroidal chamber develop a broad a distinct plateau in their temperature profile around the region of heating [15]. If heat is then deposited at positions that correspond to the two edges of this plateau, sharp peaks in the temperature profile develop at the plateau edges [15]. These features are known as "ears" and represent increased plasma confinement. It was attempted to recreate this phenomenon with the *Chapman et al.* model, again to see whether this complicated behaviour could be recovered from the sandpile model. The most impressive results were obtained by fuelling at two cells simultaneously, representative of heating the plasma at positions corresponding to the plateau edges. Clear similarities can be seen between averaged height profiles of this dual fuelling and "ears" observed experimentally (*see figure 3*).

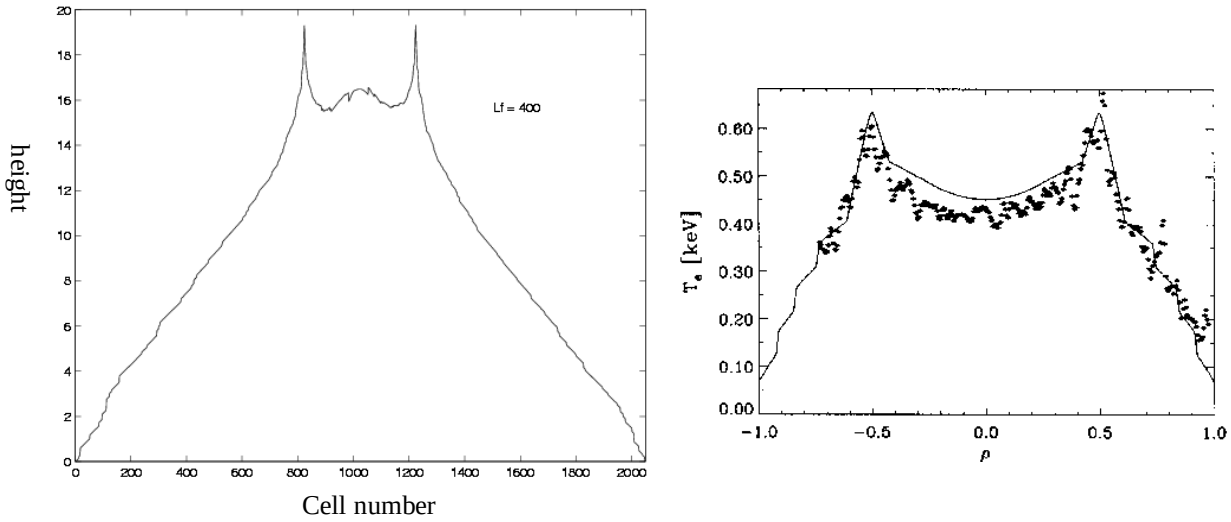

Figure 3: (Left) Average height profile of sandpile fuelled at two cells simultaneously. "Ears" can be seen as sharp peaks at the edge of the central plateau. $\boldsymbol{L_f = 400}$.

(Right) After M. R. de Baar *et al.Phys. Plasmas.* ***6****(12) 4645 (1999). Figure shows the time averaged electron temperature profile, as electron energy,* $\boldsymbol{T_e}$*, against radial displacement within the toroidal chamber* ρ*. "Ears" can be seen as peaks at approximately* $\rho = \pm 0.5$.

All the results shown thus far are produced from the original redistribution rules. Early efforts at obtaining accurate statistics for runs with $\boldsymbol{L_{for}}$ larger than 4 proved difficult because very long term saw-tooth periodicity was introduced into the energy time series of the sandpile making it difficult to judge whether the pile had indeed reached a quasi steady state. The approach of a quasi steady state in the energy time series is used to estimate the approach of the system to the critical state [14]. Statistics of avalanche length distributions from runs with $\boldsymbol{L_{for}}$ up to 4 did not deviate significantly from each other, suggesting that changes in $\boldsymbol{L_{for}}$ will not result in the adoption of another fixed point in RG space leaving $\boldsymbol{L_f}$ as the sole control parameter. However, only a limited fraction of $\boldsymbol{L_{for}}$ space has been explored. Animations of the instantaneous height profile were made of simulations with $\boldsymbol{L_{for}} > 1$. They revealed that although the height profile for runs with different values of $\boldsymbol{L_{for}}$ may vary considerably at any given time, the formation of "steps" and plateaus remains a constant feature of their phenomenology.

2.2 Modelling the Dynamics of Drops on Glass

2.2.1 Introduction

The dynamics of fluid droplets was one of the systems earmarked for investigation with regards to SOC when the concept was first introduced [1]. Despite the enormous amount of research undertaken concerning droplet dynamics [16], there is relatively little literature about experimental investigations on this subject. Two papers have been found whose topics are directly concerned with such experiments [17][18]. A discussion of their principle findings can be found in *Jenson p23.* A notable difference in their conclusions is that B. Ploude suggests power law scaling exists in the sizes and life times of drops leaving the system, where as I. M. Janosi finds no evidence to support the notion of power-law scaling. Neither experiment probed the elementary redistribution events in their search for power-law scaling relations

The aim of this investigation was to develop a cellular automater model for the dynamics of water droplets on a "glass-like" surface. The ideas of threshold driven diffusion and fluid transport were to be central in the development of a model that could exhibit SOC. The search for SOC was primarily concerned with identifying power law scaling amongst elementary redistribution events. Investigations to compare the statistics of the model with existing experimental data were also undertaken to give an idea of its physical validity.

2.2.2 Model Development

An important extension that had to be made to the *Chapman et al.* model was to make mass transport threshold driven when a drop is flowing onto dry surface (i.e. it has to overcome surface tension), and for this threshold not to exist when the drop is flowing into an existing drop (i.e. the coalescence of drops is energetically favourable because of the minimisation of surface energy). Initial ideas concerned the fitting of a stream (i.e. a drop with a trail of wetted surface left behind it) to a stream profile. The distance the drop had travelled and the total mass of the stream as it coalesces with existing droplets would scale this profiles dimensions accordingly. It was decided that this behaviour could be approximated by a simple cellular approach if: all drops are considered to have the same contact area regardless of mass (all drops occupy one cell only); all wetted trails hold the same mass of fluid per unit area; and all wetted trails are the same width regardless of the size of the drop which caused them (i.e. all trails are one cell wide). The 2D grid of cells that was used for this simulation was either connected with diamond, or square geometry. If a drop is over critical mass on a diamond grid there are only two possible "child sites" it could move to. However, if the grid is connected by square geometry there are three possible child sites (*see figure 4.).*

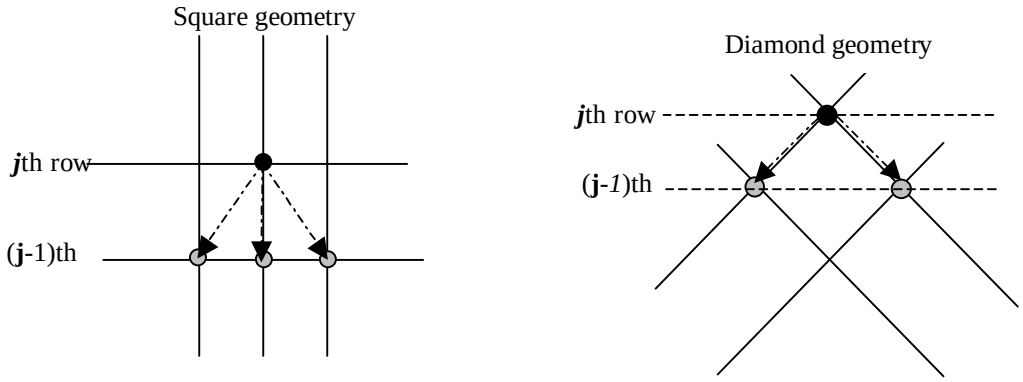

Figure 4: This figure shows two possible geometric arrangements for the 2D grid of cells used in modelling the dynamics of drops on glass. "Child sites" to the black "Parent Site" site are shown in grey. Implicitly the row index (j) decreases as the drop moves down the surface and looses gravitational potential energy

The basic algorithm is similar to that described in [18] in that, if a cell contains more than a critical amount of fluid, the following update is applied *(10a)(10b).*

$$F_p' \rightarrow \delta \qquad (10a)$$

$$F' \rightarrow F_c + F_p - \delta \qquad (10b)$$

Where F_p is the mass of water on the parent site, Fc is the mass of water on the child site and δ is the constant mass of water left behind on the parent cell due to wetting. The dashed values are to indicate they represent the mass of water after applying the relaxation, where as the un-dashed values show the original mass of water on these cells. The amount of fluid a cell needs to have before it is deemed over critical, and redistribution takes place, is governed by the rules *(11a)11(b).*

If at least one of the child sites has water, redistribution takes place to the child cell with the most water if (*11a*) is satified.

$$F_p > \delta \qquad (11a)$$

This represents non-threshold driven mass transport. The inequality condition is set so that (F_p -δ), found in *(10b)*, is never negative. A negative value of (F_p -δ) would result in water being redistributed up the pane.

If none of the child sites hold water, the cell is deemed over critical if it meets the condition:

$$F_p > c_m \qquad (11b)$$

c_m is always set to be greater than δ. Equation *(11b)* represents threshold driven diffusion – surface tension is exceeded.

If all the child sites hold the same amount of water the cell directly below the parent cell is always preferred in square geometry, and one of the two child cells is chosen at random in diamond geometry.

The same update algorithm is then applied to the child sites until the "avalanche" stops or comes to the outflow boundary at row j=0. Thus, relaxation is instantaneous. The boundaries at the sides of the grid are periodic.

The system is driven by randomly depositing droplets of size g over the grid. After each deposition the deposition site is checked for conditions *(10a)* and *(10b)*, and relaxation takes place accordingly. B. Ploude *et al.* argue that, in order to adequately describe the dynamics of water droplets consideration has to be given to droplet formation and deposition, as well as coalescence and avalanching [19]. Thus, droplets are allowed to coalesce on deposition if the parent or child sites of the deposition site have water. If two droplets coalesce in this way, the site where the smaller mass was becomes empty and the water is summed onto the site that has the larger mass. This process forms clusters with open spaces between them in an attempt to account for droplet formation on deposition.

Experimentalists also talk of droplet formation in the wetted stream left by a moving droplet. Identifying a fluidisation length, λ, simulates this. If a cell is part of a droplet's wetted stream, and is greater than λ cells from the droplet, then the water in this cell is removed and combined with that of the cell in the same stream one row above it with a probability of ½. Thus, the path of the droplet is covered by a perfectly wetted region, up to a distance λ from the avalanching droplet, and then the path is randomly interspersed with clusters and open spaces (i.e. droplets form in the wetted part of the stream).

If there is an over-critical mass of water on a cell on row j=0, outflow occurs. Here all cells that the avalanching drop has visited, within a distance λ of the boundary, are set to zero. This prevents the long term existence of large wetted regions, which if allowed to remain, would lead to transport being entirely dominated by non-threshold driven means. Outflow in this way is analogous to the "re-setting avalanches" discussed in *Jenson*.

The value of λ was allowed to fluctuate about a mean value, $<\lambda>$. This means a new value of λ was drawn from a "top-hat" probability distribution, centred around $<\lambda>$, every time the program needs a value for λ. Values for λ were allowed to fluctuate by 25% with no apparent effect on system statistics. This demonstrates some degree of robustness. Further tests for robustness will have to include the introduction of randomness in c_m .

2.2.3 Model Behaviour

The model was designed to allow non-threshold effects to play a vital role in the transport of mass, and thus act as a proxy to fluid transport. Regions of spatial correlation (streams) are produced that direct fluid transport along them. However, the lengths of these spatial correlations are limited by the formation of droplets in the wetted part of the stream and, to a lesser extent, by the formation of droplets by deposition. Streams are removed by outflow events. Maintaining a balance between the formation and destruction of spatial correlations was found to be crucial in recovering power law scaling in avalanche length distributions, as can be seen in figure *5*, *6* and *7*. The length of an avalanche is simply defined as the difference in row number from when the drop was initially deposited to when the drop's motion is terminated, be it by becoming under-critical or by outflow.

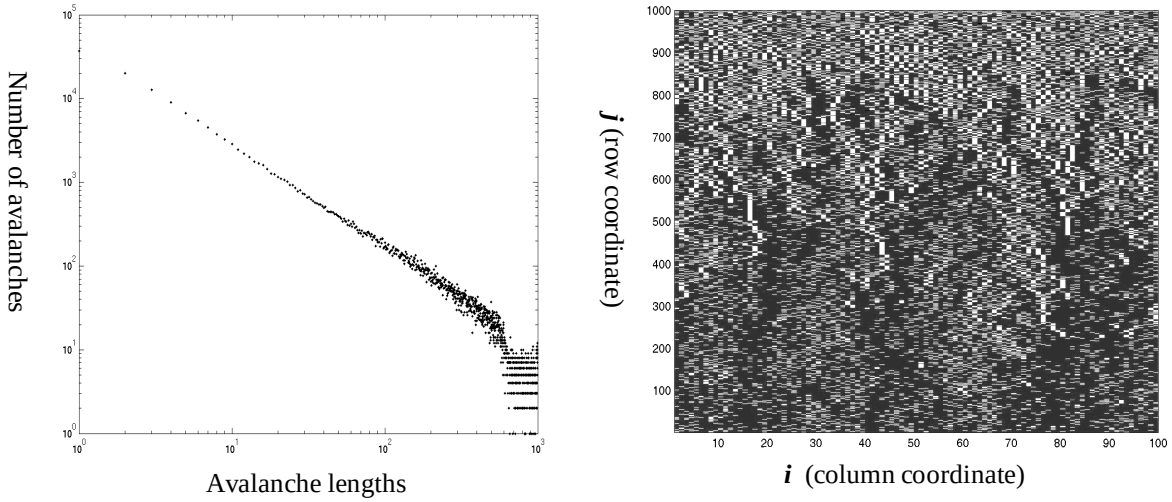

Figure 5 (Left) Plot showing the number of avalanches recorded per avalanche length. (Right) Colour map showing the amount of water in each cell after completing the simulation. Lighter shades represent more water. Here <λ> was set to 750.

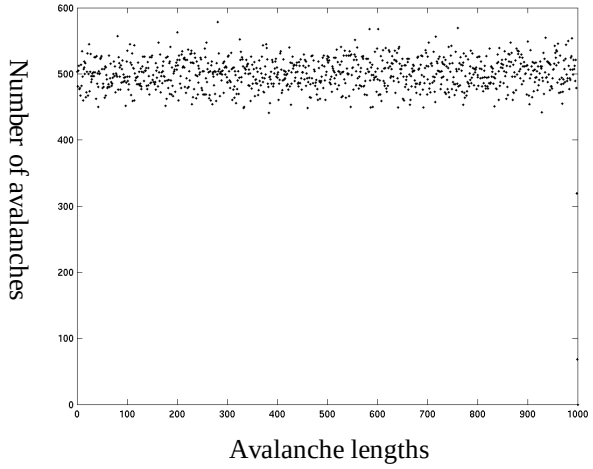

Figure 6: This simulation was run to demonstrate the effect of allowing spatial correlation to build without them being destroyed. This was done by altering the simulation so only one drop was removed on out-flow, droplets were no allowed to form on deposition and droplets were not allowed to form in the wetted part of the stream. Avalanches become equally likely for all allowed lengths. <λ> is 750.

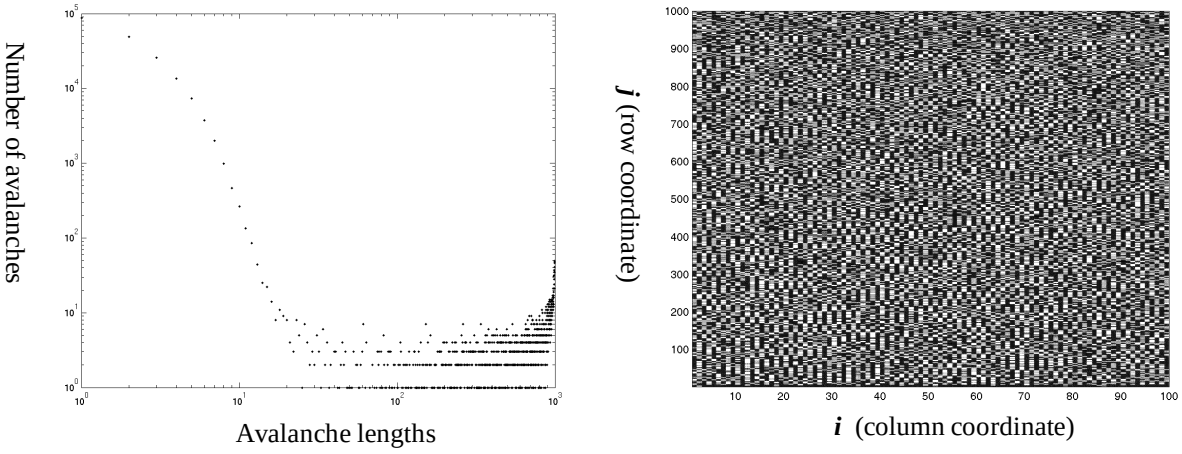

Figure 7: (Left) Plot showing the number of avalanches recorded per avalanche length. (R ight) Colour map showing the amount of water in each cell after completing the simulation. This simulation was run to demonstrate the effect of restricting the length of spatial correlations to a length much smaller than the number of rows in the grid (i.e. here <λ> is 5*).*

All the runs for figures *5*, *6* and *7* where performed on a grid of 100 by 1000 cells with square geometry, g was 10, c_m was 100 and δ was 12. Figure *5* shows power law scaling of avalanche lengths over nearly three decades (obviously the number of decades over which this scaling can take place is limited by the system size). The colour map of figure *5* shows well defined streams which exist over hundreds of cells. Figure *6* shows a "white" distribution of avalanche lengths, the data in this figure has been plotted linearly for clarity. This "white" distribution is the result of allowing spatial correlations to form but not introducing methods to destroy them. The colour map would show a homogenous grid with every cell holding δ. Every deposition would lead to an avalanche stretching to the open boundary because of condition *(11a)*. Figure *7* shows that the power law scaling for avalanche lengths is all but destroyed when spatial correlations are limited to a value far smaller than the number of rows in the system. The colour map shows the absence of the large streams, which are visible in figure *5*.

These figures show that the formation of streams is important in creating power law scaling over a wide range of avalanche lengths, and that mechanisms that disrupt the formation of streams are important in preventing the avalanche length distribution from becoming saturated by fluid transport avalanches.

The model's behaviour was checked for consistency with experimental results shown in [17]. Figure *8* shows avalanche length distribution for two values of δ the experimental results from [17].

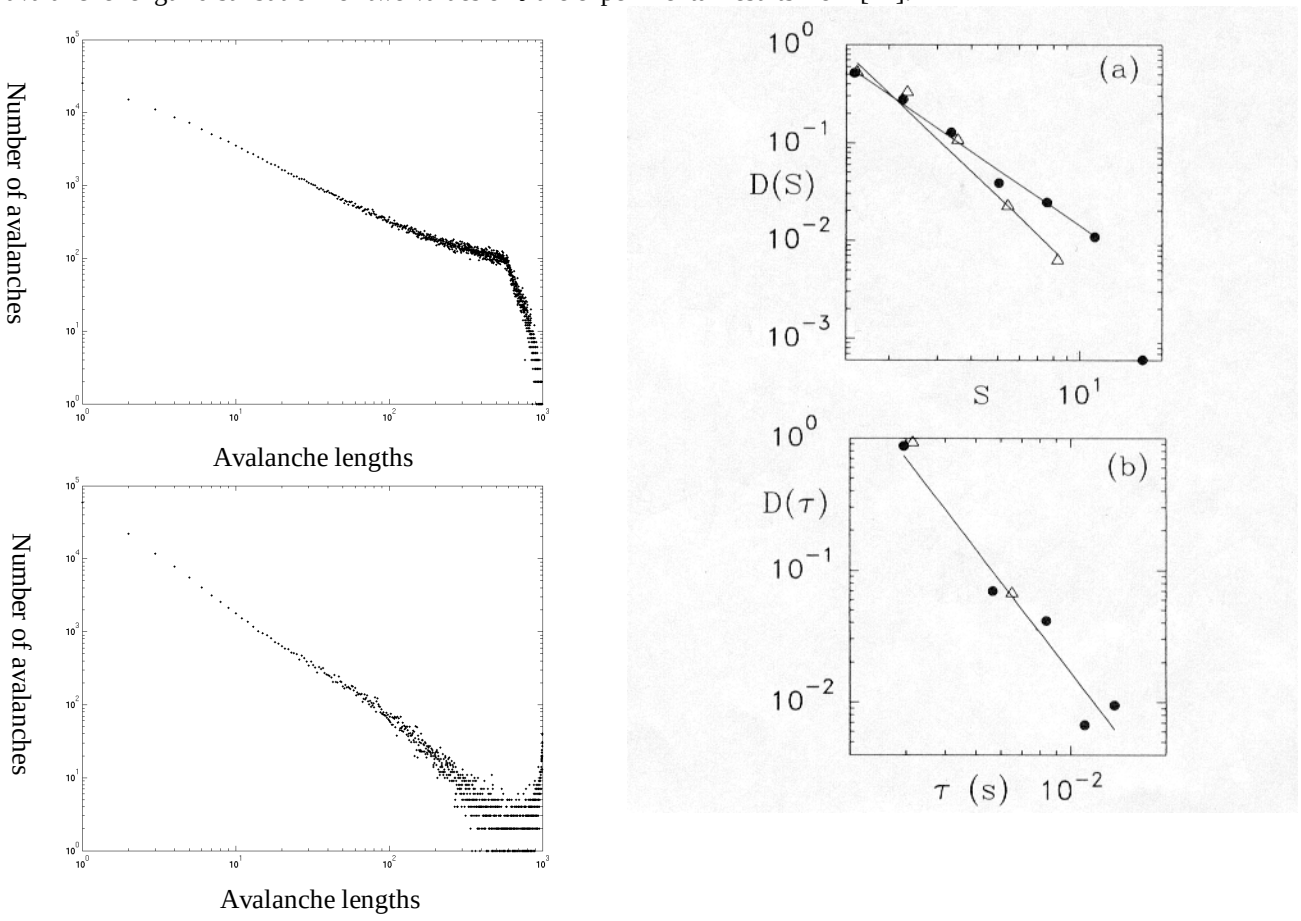

Figure 8:.(Left, Top) Plot of number of avalanches against avalanche lengths. δ is 40. (Left, Bottom) Plot of number of avalanches against avalanche lengths. δ is 4. A different critical exponent defines the power law scaling for each case. Increasing δ can be seen as a proxy to increasing the viscosity of the fluid.

*(Right) After B Ploude et al. Phys. Rev. Let **71**(17) 2749 (1993). Figure (a) show the probability density distribution, D(S), of drops size, S. Figure (b) shows the probability density distribution of, D(τ), of the time stamps of outflow events, τ. Since relaxation and ouflow is instantaneous in the model discussed in this paper, no measurements could be made appropriate for comparison with this data. Triangular markers are used for the high temperature (low viscosity) case and circular markers are used for the low temperature, (high viscosity) case.*

It needs to be noted that a direct comparison cannot be drawn between the results shown in [17] and those displayed in figure *8*. This is because *B. Ploude et al.* measured the statistics of out-flow events only (specifically the distribution of out flow masses for which evidence of power law scaling was found) where as the graphs displayed in figure *8* concern the internal events of the system and deal in avalanche lengths, not outflow masses. Power law scaling does not exist for the simulated out flow masses. The distribution of simulated outflow masses is usually peaked around a preferred mass. If a comparison between the graphs in figure *8* and the results in [17] is made (*see figure* 8) it can be seen that both exhibit power law scaling in there distributions and both show an increase in the critical exponent (α) with increased viscosity. Increasing δ act acts a proxy to increasing viscosity. The simulated outflow mass distributions are distorted from experimental ones because of the mechanism used in the simulation. Simulated outflow events involve the removal of all water in the fluid stream within a distance of λ cells from the open boundary. In practice this would not be seen as one event but the water would leave the system through a "dripping" process. *B. Ploude et al.* make an attempt to identify drips that are causally related, and so sum them into one outflow event. It is unlikely that the removal of the entire wetted region of the fluid stream will be identified as one outflow event in this way since drips separated by more than 7msec were not considered to be causally connected.

The number of deposition iterations can be thought of as a linear indication of time, since relaxation is assumed to be instantaneous. The delay times between successive outflow events, Δt, were always found to have a probability distribution that decayed with an exponential dependence for all cases investigated. Steeper decays were found for higher deposition rates (larger values of g), as shown in figure *9*.

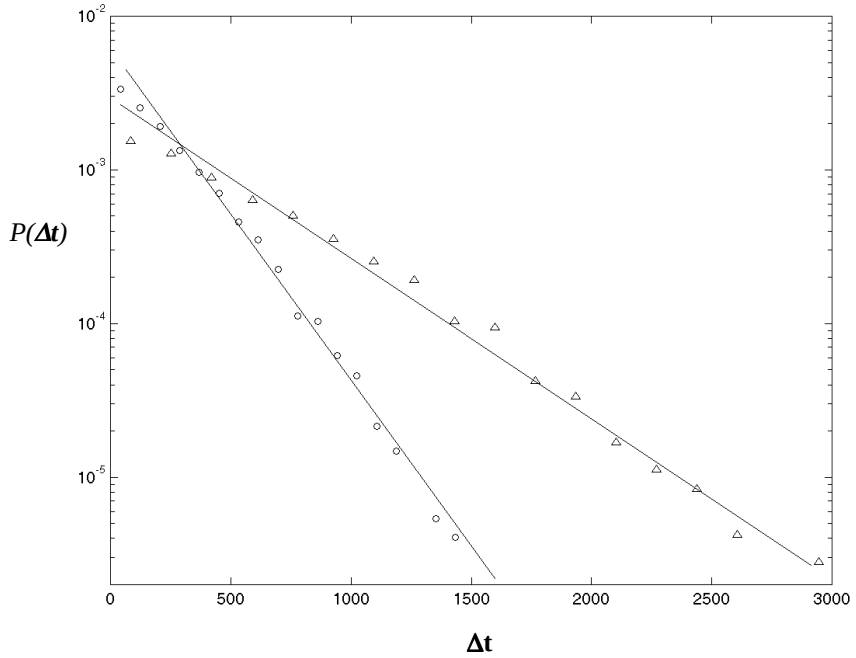

Figure 9: Probability density distribution of outflow delay times for two different values of g. *(circles)* g *is 20, (triangles)* g *is 10. The grid was composed of 1000 rows and 100 columns in both cases. .* $\langle\lambda\rangle$ was 750, δ was 8 and c_m was 100. *P(*Δt*) was calculated by binning the data linearly.*

Ploude et al. also produced return maps of delay times between outflow events to determine whether there was significant correlation between successive outflow events. The return maps produced in [17] (see *figure 10)* show a high triangular concentration of events around the origin. *B Ploude et al.* explained that the more diffuse distribution, produced for a low deposition rate, was due to the broadening of the delay time distribution as the deposition rate is decreased. The simulated return maps were found to become more diffuse, and the distributions of delay times were found to become broader, as g was decreased (see figures *10* and *9* respectively). This is in agreement the finding of *B. Ploude et al.*

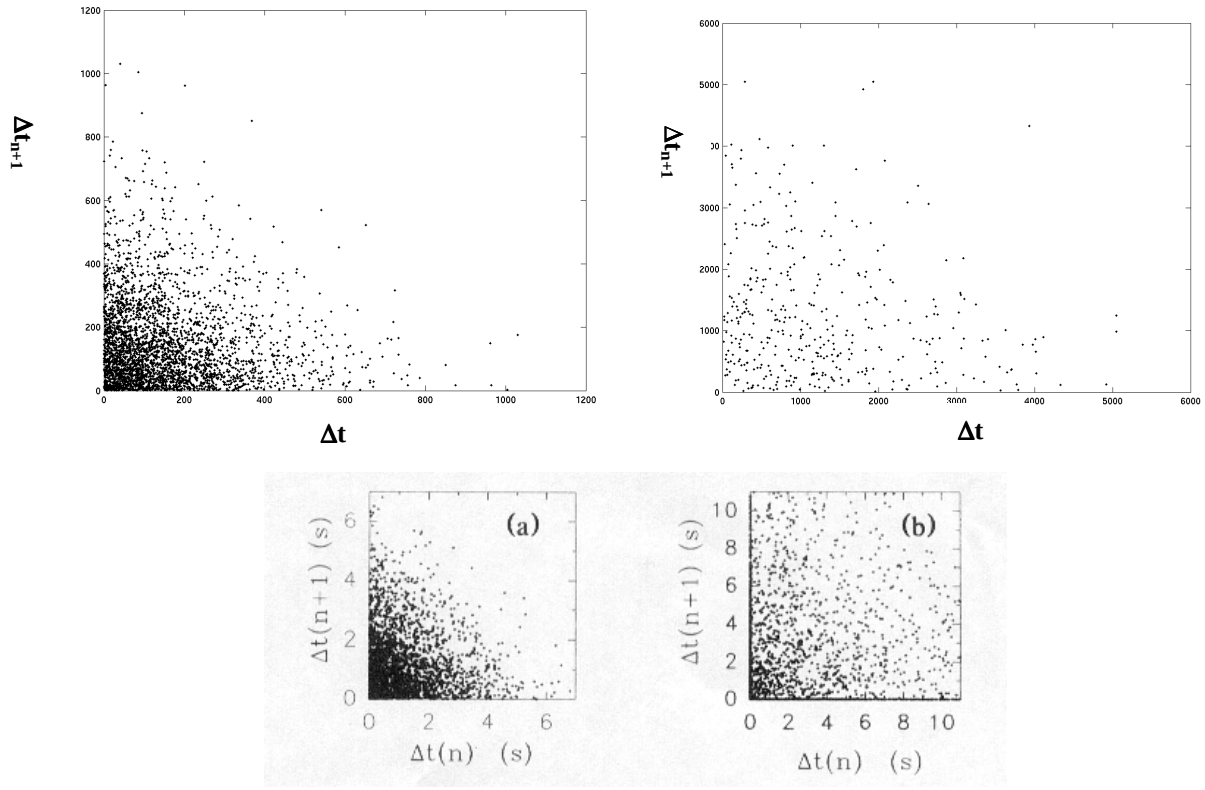

Figure 10: Return maps of Δt_{n+1} versus Δt_n for: (Top Left) high deposition rate data ($g = 40$), and (Top Right) low deposition rate data ($g = 10$)

*(Bottom) After Plourde et al. Phys. Rev. Let **71**(17) 2749 (1993). Return maps of data collected at high viscosity for a high flow rate (a), 17cm^3/min, and a low flow rate (b), 8cm^3/min*

The task of extracting data from the simulation, which could be tested experimentally, was also addressed. Probing the elemental redistribution events in the system is considered most important in determining whether it had evolved into a critical state. The gravitational potential energy dissipated in each avalanche event was probed for power-law scaling. The potential energy of the system, E_g, was simply identified by equitation *(12).*

$$E_g = \sum_{i=1}^{w} \sum_{j=0}^{(h-1)} jF_{j,i} \qquad (12)$$

Where w is the number of columns in the grid and h is the number of rows. In this simple approach, gravitational potential energy scales linearly with fluid mass and row index. Increasing the row index implies moving up the inclined surface. It is imagined that a video recording could be made of the inclined surface as the experiment is run, as in [18], and then image processing could be used to identify how much water is resting on a cellular region for desecrate time intervals. Assuming it could be determined at what time an avalanche started and stopped, energy dissipation statistics could then be recovered. An example of simulated avalanche energy dissipation is shown in figure *11*

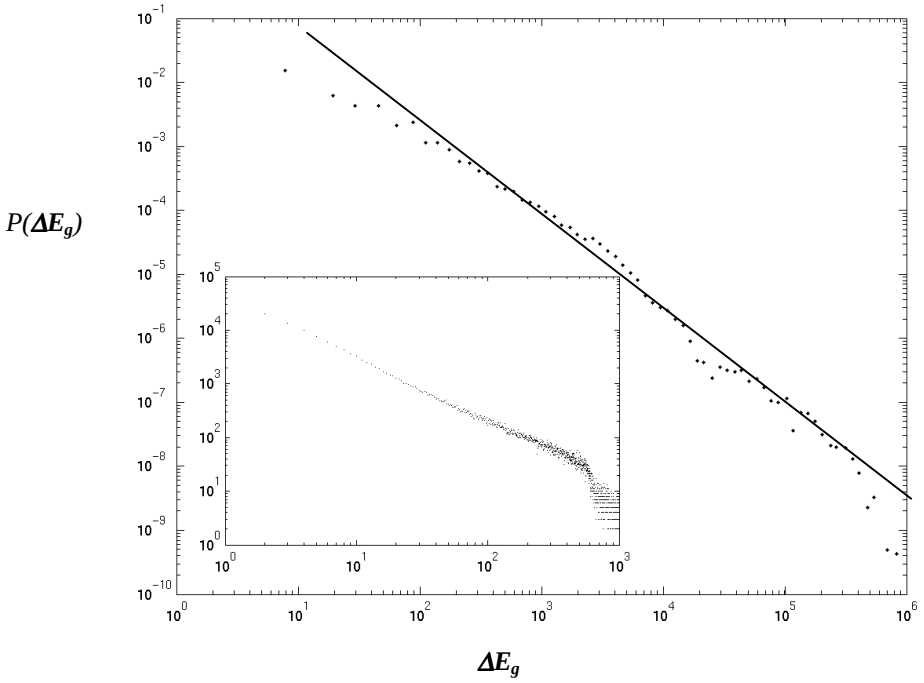

Figure 11: Plot showing probability density distribution of simulated avalanche energy dissipation of system with g = 12, δ = 16, $\langle\lambda\rangle$ = 750 and c_m was 100. The grid had 1000 rows and 100 columns. Evidence of power law scaling can be seen. Inset is the avalanche length distribution for the same run. Number of avalanches is shown on the abscissa and avalanche length is shown on the ordinate axis. $P(\Delta E_g)$ was calculated by binning the data logarithmically.

It is not clear if a definite relation exists between avalanche length scaling and energy dissipation scaling. This requires further investigation. An obvious advantage of studying energy dissipation is that events are recorded on a range decades larger than that of avalanche lengths.

Time series of simulated surface coverage, as investigated in [18], and of the net mass on the surface, as investigated in were taken. There spectral power densities were estimated using *Matlab's* "psd" command. Both power spectrums were found to decay as $1/f^2$ (where f represents frequency).

Grids with square geometry were used to produce all the results shown in this section, as was used in [18]. Results collected using both geometries appeared to demonstrate the same phenomenology, although the precise effect of the different geometries on the statistics of the simulation was not determined.

3. Discussion

The models described in section **2** use a reduced physics, rather than a full numeric simulation, to investigate complex behaviour. Crucially, these models are concerned with characterising behaviour on spatial and temporal scales, which are large in comparison to elementary interactions. This macroscopic approach has paid dividends in the past by virtue of the law of large numbers and the central limit theorem (e.g. Navier Stokes equation describes fluid motion without considering particular collisions). In cases like this, microscopic fluctuations are averaged out. In other systems this approach is not possible since the details of the interactions on all scales are important in explaining the behaviour of the system. In this case a full numerical simulation is required. In between these two cases lies the regime in which fluctuation are not averaged out entirely, but lead to self similarity over many decades, so the *details* of interactions on all scales need not be considered [20].

With this in mind, the models must be designed to include the symmetry and scaling of the physical system. It is also essential that these models are robust against fluctuations and can recover the same dynamics when given a range of parameters. If it is asserted that the behaviour of the systems being modelled is not a consequence of its microscopic details, then the behaviour of the models should not depend on their details (i.e. the fine tuning of parameters). An RG analysis has been performed on the sandpile of *Chapman et al.* [13]. This recovered a

scaling of avalanche frequency with avalanche size (α=1) that corresponds to a fixed point. This fixed point shows the scaling should be robust to fluctuations - a result confirmed numerically. An RG analysis has not been performed for the droplet dynamics model but a range of deposition rates values of c_m have been explored. Two geometries for the lattice sites were also investigated. The fact that the frequency of delay times always decayed exponentially with magnitude and the frequency of avalanches always decayed as a power law with magnitude, appears to be the robust behaviour of the model. Of course, all areas of parameter space have not been explored for this model; the extent of its robustness cannot be determined until an analytic solution is found.

The error bars shown have been calculated by taking the reciprocal of the square root of the number events recorded in a particular bin. This is taken as an estimate of uncertainty. In figures *9* and *11* there are deviations from straight-line behaviour. This may be because the system size used (only 100x1000 cells) was not large enough to view events of the magnitude that this approach is applicable to. However, conclusions drawn based on the projection of this data onto the straight-line fit should be viewed with this deviation in mind.

4. Conclusion

The results presented in section **2.1.3** show that a few simple modifications can be made to the *Chapman et al.* model to reproduce some characteristic phenomenology of the temperature profiles of tokamak confined plasmas. This builds on the ideas presented in [7][8][9][10] that link sandpile models to tokamak confinement. Further investigations are required to determine the extent to which these models can be used to quantitatively simulate fusion experiments and if an accurate predictive model can be made. These developments will help to confirm tokamak plasma confinement as being a physical realisation of SOC.

The results presented in section **2.2.3** show that a simple model for the dynamics of drops on an inclined glass-like surface, which demonstrates power law scaling for elementary redistribution events, can be made. Two aspects of the model were identified as critical to the recovery of this power law scaling. Firstly, macroscopic regions of wetting ("streams") must be allowed to exist on scales similar to that of the system, and secondly, a mechanism must exist that destroys the special correlation in these streams (here droplet formation) and streams must be allowed to be removed from the system quickly once they have joined with the outflow boundary.

Experimentalists can estimate the effect of droplet formation on destroying the correlation in the wetted stream by measuring the contact angle of a droplet with the glass. From this a wetting time is estimated – streams are destroyed by droplet formation in this characteristic time. In [18] a glass with a very low wetting time was chosen to restrict the formation of macroscopically wetted regions. It has to be noted that droplet formation was associated with a characteristic distance, λ, in the model and not a characteristic time. There is also the question as to whether the outflow algorithm applied in this model, vital in destroying streams connected to the open boundary, is physically applicable to real droplet dynamics.

The model is successful in reproducing the qualitative statistical behaviour of outflow times shown in figures *9* and *10*, which have been found experimentally [17]. Further investigations into the physical applicability of the algorithm (such as that suggested to test the prediction shown in figure *11*) need to be made to determine whether the dynamics of water droplets is a physical realisation of SOC.

Bibliography

Jenson H. J. Jensen "Self-Organised Criticality Emergent Complex Behaviour in Physical and Biological Systems" Cambridge University Press 2000

Sornette D. Sornette "Critical Phenomena in Natural Sciences Chaos, Fractals Self-Organization and Disorder: Concepts and Tools" Springer London 2000

References

[1]P. Bak, C. Tang and K. Wiesenfield, Phys. Rev. Lett. **59,** 381 (1987); Phys Rev A **38**, 364 (1988)

[2] D. Sornette "Critical Phenomena in Natural Sciences Chaos, Fractals Self-Organization and Disorder: Concepts and Tools" Springer London 2000, **p 299**

[3] H. Fellerman http://www.-lehre.informatik.uos.de/~hfellerm/stadium/SOC/SOC.html "Introduction to Self-Organised Criticality" last updated 13/11/2000 last visited 29/12/2001

[4] D. Sornette "Critical Phenomena in Natural Sciences Chaos, Fractals Self-Organization and Disorder: Concepts and Tools" Springer London 2000, **p 40 & 225**

[5] Fusion Power - UKAEA Fusion at Culham http://www.fusion.org.uk/ last visited 8/01/2002

[6] J. Pamela, E. R. Solano "From JET to ITER: Preparing the Next Step in Fusion Reasearch" JET EFDA CSU, Culham Science Centre, Abingdon, OX14 3EA, U.K.

[7] D. E. Newman, B. A. Carreras, P. H. Diamond, and T. S. Hahm, Phys. Plasmas **3**, 1858 (1996)

[8] B. A. Carreras, D. E. Newman and V. E. Lynch, Phys. Plasmas **3,** 2903 (1996)

[9] P. A. Politzer, Phys. Rev. Lett. **84,** 1192 (2000)

[10] S. C. Chapman, R. O. Dendy and B. Hnat, Phys. Rev. Lett. **86**(13) 2814 (2001)

[11] S. C. Chapman, R. O. Dendy and B. Hnat, Phys. Plasmas **8**(5) 1969 (2001)

[12] P. Helender, S. C. Chapman, R. O. Dendy, G. Rowlands and N. W. Watkins, Phys. Rev. E **59**(6) 6356 (1999)

[13] Sunny W. Y. Tam, Tom Chang, S. C. Chapman and N. W. Watkins Geophys. Research Letters **27,** 1367 (2000)

[14] S.C. Chapman, Phys. Rev. E **62**(2) 1905 (2000)

[15] M. R. de Baar, M. N. Beurskens, G. M. D. Hogweij, and N. J. Lopes Cardozo, Phys. Plasmas, **6**(12) 4645 (1999)

[16]A.M, Cazabat, Contemp. Phys. **28,** 347 (1987) [GET]

[17] Britton Plourde, Franco Nori and Michael Bretz Physical Review Letters **71** 2749 (1993)

[18] Imre M. Janoisi an Victor K. Horvath, Phys. Rev. A, **40**, 5232 (1989)

[19]Britton Plourde, Franco Nori and Michael Bretz Physical Review Letters **74**(17) 3498 (1995)

[20] James P. Sethna, Karin A. Dahmen, and Christopher R. Myers, Nature **410** 242-250 (2001)